Cell & Bioscience

https://doi.org/10.1186/s13578-026-01569-0

Article in Press

Overexpression of ONECUT1 suppresses hepatoblastoma progression via modulating tumor cell growth and tumor microenvironment

Received: 11 November 2025

Accepted: 18 March 2026

Published online: 05 April 2026

Cite this article as: Qiao Y., Xu M., Wu Y. *et al.* Overexpression of ONECUT1 suppresses hepatoblastoma progression via modulating tumor cell growth and tumor microenvironment. *Cell Biosci* (2026). https://doi.org/10.1186/s13578-026-01569-0

Yu Qiao, Meng Xu, Yanhui Wu, Guofei Cui, Shanshan Deng, Liangliang Bai, Xiaoshuang Song, Jian Zhong, Weijie Bian, Gang Yu, Matthias Evert, Xue Wang, Diego F. Calvisi, Xin Chen, Lin Li & Weiting Liao

Overexpression of ONECUT1 suppresses hepatoblastoma progression via modulating tumor cell growth and tumor microenvironment

Yu Qiao[† 1.2], Meng Xu[† 2.3], Yanhui Wu[2.4.5], Guofei Cui[2], Shanshan Deng[2], Liangliang Bai[6], Xiaoshuang Song[7], Jian Zhong[8], Weijie Bian[8], Gang Yu[9], Matthias Evert[10], Xue Wang[2], Diego F. Calvisi[10], Xin Chen[2*], Lin Li[1*], Weiting Liao[2,6*]

[1]Department of Medical Oncology, Beijing Hospital, National Center of Gerontology, Institute of Geriatric Medicine, Chinese Academy of Medical Sciences & Peking Union Medical College, Beijing 100730, China.

[2]Cancer Biology Program, University of Hawaii Cancer Center, Honolulu, Hawaii 96813, USA.

[3]Department of General Surgery, The Second Affiliated Hospital of Xi'an Jiaotong University, Xi'an, Shaanxi 710004, China.

[4]Division of Hepato-Pancreato-Biliary Surgery, Tongji Hospital, Tongji Medical College, Huazhong University of Science & Technology, Wuhan, Hubei 430030, China.

[5]Hubei Key Laboratory of Hepato-Pancreato-Biliary Diseases, Wuhan, Hubei 430030, China.

[6]Department of Medical Oncology, Cancer Center, West China Hospital, Sichuan University, Chengdu, Sichuan 610041, China.

[7]Department of Biotherapy, State Key Laboratory of Biotherapy and Cancer Center, Collaborative Innovation Center of Biotherapy, West China Hospital, Sichuan University, Chengdu, Sichuan 610041, China.

[8]Peking University ChengDu Academy for Advanced Interdisciplinary Biotechnologies, Chengdu, Sichuan 610213, China.

[9]Beijing Municipal Bureau of Retired Cadre Service, Beijing 100034, China

[10]Institute of Pathology, University of Regensburg, Regensburg 93053, Germany.

[†] Yu Qiao and Meng Xu contributed equally to this work.

*Xin Chen, Lin Li, and Weiting Liao are co-corresponding authors.

Corresponding authors: Xin Chen, Cancer Biology Program, University of Hawaii Cancer Center, 96813, Honolulu, Hawaii, USA. Email: xinchen3@hawaii.edu. Lin Li, Department of Medical Oncology, Beijing Hospital, National Center of Gerontology, Institute of Geriatric Medicine, Chinese Academy of Medical Sciences & Peking Union Medical College, Beijing 100730, China. Email: lilin_51@hotmail.com. Weiting Liao, Department of Medical Oncology, Cancer Center, West China Hospital, Sichuan University, Chengdu, Sichuan 610041, China. Email: liaoweitingl@163.com.

List of Abbreviations:

α-SMA	Alpha-Smooth Muscle Actin
CC3 (Cl. Caspase-3)	Cleaved Caspase-3
CCL20	C-C Motif Chemokine Ligand 20
CDK	Cyclin-Dependent Kinase
CXCL16	C-X-C Motif Chemokine Ligand 16
DOX	Doxycycline
EMT	Epithelial–Mesenchymal Transition
F4/80	Macrophage Marker F4/80
HB	Hepatoblastoma
H&E	Hematoxylin and Eosin

HLA	Human Leukocyte Antigen
ONECUT1	One Cut Homeobox 1
HTVI	Hydrodynamic Tail Vein Injection
IHC	Immunohistochemistry
IL16	Interleukin-16
MHC-I	Major Histocompatibility Complex Class I
NSG	NOD/SCID/IL2Rγnull Mice
PI	Propidium Iodide
qRT-PCR	Quantitative Reverse Transcription Polymerase Chain Reaction
SB	Sleeping Beauty Transposase System
YAPS127A	Constitutively Active YAP Mutant (Serine 127 → Alanine)
ΔN90-β-catenin	N-terminally Truncated β-catenin

Conflict of interests: Nothing to disclose.

Acknowledgments: We appreciate Professor Hongxin Deng (Department of Biotherapy, Cancer Center, and State Key Laboratory of Biotherapy, West China Hospital, Sichuan University, Chengdu, China) for his valuable support. We also extend our gratitude to Professor Sisi Wu, Jiangrong Deng, Shuaishuai Yu, Jinhan Zhou, Shuxia Zhang, Xiaojiao Wang, Dan Luo and Xin Luo (Core Facilities of West China Hospital, Sichuan University, Chengdu, China) for their assistance.

Funding: This study was supported by National Institutes of Health (grant numbers R01 CA228483, R01 CA239251, and R01 CA250227), Postdoctoral Fellowship Program of China Postdoctoral Science Foundation (GZB20250508 and 2025M772115), Postdoctor Research Fund of West China Hospital, Sichuan University (2025HXBH024), Natural Science Foundation of Sichuan Province (2026NSFSC1938) and CAMS Innovation Fund for Medical Sciences (CIFMS) (grant numbers 2024-I2M-C&T-B-093).

Abstract

Background:

Hepatoblastoma is the most common malignant liver tumor in children. Our previous work showed that enforced expression of the transcription factor One Cut Homeobox 1 (ONECUT1) suppresses the initiation of hepatoblastoma. However, it remains unclear whether increasing ONECUT1 expression can also inhibit tumor progression after tumors have already formed. The purpose of this study was to determine the effects of ONECUT1 induction on tumor cell behavior and tumor growth during established hepatoblastoma progression.

Results:

We generated doxycycline-inducible expression systems to upregulate ONECUT1 in hepatoblastoma cells in culture and in mouse models. In human hepatoblastoma cells, induction of ONECUT1 promoted apoptotic cell death and reduced cell cycle progression. In a subcutaneous xenograft model using immunodeficient mice, ONECUT1 induction slowed tumor growth but did not cause tumor regression. We then established an orthotopic HB model in *FVB/N* mice by tail-vein injection of *YAP/β-catenin/TRE-ONECUT1* plasmids. ONECUT1 expression in existing mouse HB cells was induced by feeding the mice with DOX-water. Remarkably, tumor regression was observed following ONECUT1 induction. Histological analyses showed extensive necrosis and apoptosis in tumor lesions following induction of ONECUT1, accompanied by robust macrophage infiltration and moderate T cell infiltration. Depletion of T cells using antibodies against CD4 and CD8 weakened the antitumor effect of ONECUT1, indicating that T-cell activity contributes to tumor suppression. Transcriptomic analysis further suggested that ONECUT1 may promote antitumor immune responses in part by increasing expression of immune-related cytokines.

Conclusions:

Induction of ONECUT1 suppresses hepatoblastoma progression by inhibiting tumor cell growth and by reshaping the tumor immune microenvironment. These findings reveal a previously

unrecognized antitumor role of ONECUT1 during hepatoblastoma progression and suggest that restoring ONECUT1 activity may represent a promising therapeutic strategy for this pediatric malignancy.

Keywords: Hepatoblastoma; ONECUT1; CXCL16; Tumor Immune Microenvironment

Introduction

Hepatoblastoma (HB) is the most common primary liver tumor in children, making up about 1% of all pediatric cancers, and is typically diagnosed in children younger than three years of age. Although its incidence is relatively low, estimated at 1.5 cases per million children worldwide, epidemiological studies suggest a gradual increase in recent decades[1, 2]. The etiology of HB remains incompletely defined, but several risk factors have been identified, including prematurity, very low birth weight, and genetic predisposition syndromes such as Beckwith–Wiedemann, Simpson-Golabi-Behmel, familial adenomatous polyposis, and trisomy 18[1, 3, 4]. At the molecular level, aberrant activation of the Wnt/β-catenin pathway and dysregulation of Hippo-Yes-associated protein (YAP) signaling are frequently observed in HB and are believed to play central roles in tumor initiation and progression[5]. Therapeutic management of HB primarily involves surgical resection in combination with cisplatin-based chemotherapy. These interventions have improved overall survival, reaching nearly 80% in patients with standard-risk disease[6, 7]. However, outcomes remain poor in those with unresectable, metastatic, or chemo-resistant tumors, and chemotherapy-related toxicities remain significant clinical challenges. Despite these clinical advances, the underlying molecular and immunological mechanisms that govern HB development and therapeutic response remain largely unclear, limiting the identification of effective and less toxic targeted therapies[1].

YAP and β-catenin represent two critical oncogenic pathways in HB. Exon-3 deletions or missense mutations in the CTNNB1 gene are detected in approximately 80–90% of HB cases, driving aberrant Wnt signaling and uncontrolled cell proliferation[8]. Concurrently, nuclear accumulation of YAP, a key effector of Hippo signaling, is frequently observed in HB[9]. Functional studies in murine models demonstrate that co-activation of YAP and β-catenin synergistically

induces HB initiation and progression[9]. These findings highlight their cooperative role in HB pathogenesis and their potential as therapeutic targets.

One cut homeobox 1 (ONECUT1, also known as HNF6) is a transcription factor involved in liver development, differentiation, and metabolism[10]. Several studies have reported conflicting roles of ONECUT1 in cancer progression. A study suggested that ONECUT1 promotes tumor growth in colorectal cancer and enhances liver metastasis in mouse models[11]. Other studies indicated instead that ONECUT1 may have tumor-suppressive roles. For instance, ONECUT1 suppresses the migration and invasive growth of lung cancer cells through p53 activation and inhibition of epithelial-mesenchymal transition (EMT)[12], and loss of ONECUT1 expression correlates with pancreatic cancer progression[13]. Moreover, ONECUT1 inhibits the growth and metastasis of cholangiocarcinoma cells by regulating miR-122[14]. In our previous investigation, we showed that ONECUT1 overexpression strongly inhibits HB initiation in the YAP/β-catenin driven murine HB model[15]. However, it remains unknown whether enforced ONECUT1 expression in established HB is sufficient to induce tumor regression. This question is important as it has key implications for the (re)activation of the ONECUT1 pathway for HB treatment.

In this study, we determined whether the overexpression of ONECUT1 suppresses the progression of HB. To achieve this purpose, we created a Doxycycline (DOX) inducible construct for ONECUT1. Subsequently, we induced the expression of ONECUT1 both *in vitro* and *in vivo* using HepG2 xenografts, as well as a YAP/β-catenin-driven murine model of HB. Our findings demonstrate that the overexpression of ONECUT1 significantly inhibits HB progression by reducing cell proliferation and promoting cell death. Additionally, our investigation emphasizes the crucial role of the immune system in this process. Overall, these data provide a mechanistic

understanding and support the development of ONECUT1-based interventions as a promising strategy against aggressive HB.

Materials and Methods

Plasmids and Reagents

The plasmids used for hydrodynamic tail vein injection in mice included pT3-EF1α-MYC-ΔN90-β-catenin, pT3-EF1α-Flag-YAPS127A and TRE empty vector which have been previously described[15, 16]. The pCMV(CAT)T7-SB100 vector was generously provided by Dr. Xinjun Lu (Zhongshan University, Guangzhou, China). The open reading frame (ORF) cDNA of ONECUT1 (Product ID: T7446) was obtained from GeneCopoeia, Inc. (Rockville, MD). PCR amplification of ONECUT1 was performed using the following primers: BamHI forward (CGA CTG GAT CCA TGA ACG CGC AGC TGA C) and EcoRI reverse (GCC GCG AAT TCT CAT GCT TTG GTA CAA GTG C). PCR products were purified using the DNA Clean & Concentrator™-5 Kit (Zymo Research, Irvine, CA). Both the amplified ONECUT1 fragment and the Gateway™ pENTR vector were digested overnight with BamHI and EcoRI, followed by electrophoresis on a 1% agarose gel. The desired DNA bands were extracted with the Zymoclean™ Gel DNA Recovery Kit (Zymo Research). Ligation of the purified insert and vector resulted in the pENTR-ONECUT1 construct, which was validated by Sanger sequencing. The Gateway LR Clonase™ II Enzyme Mix (Invitrogen) was subsequently used to recombine pENTR-ONECUT1 into destination vectors, generating pINDUCER20-ONECUT1 and TRE-ONECUT1-PGK-rTTA. The pINDUCER20 backbone (Addgene plasmid #44012) was obtained from Addgene. All final plasmid preparations were carried out using the ZymoPURE II Plasmid Maxiprep Kit (D4203, Zymo Research, Irvine, CA).

Cell culture

HepG2 and Huh6 cell lines were maintained in Dulbecco's Modified Eagle Medium (DMEM) supplemented with 10% fetal bovine serum (FBS) and 1% penicillin-streptomycin (P/S). The cells were cultured at 37 ° C in a humidified atmosphere containing 5% CO_2.

Lentivirus packaging and cell transfection

Lentivirus packaging and cell transfection were performed as described previously[17]. Briefly, early-passaged HEK-293FT cells were cultured in DMEM (without PS) at 37 ° C, 5% CO_2, seeded in 6-well plates, and transfected at 60-70% confluence with a plasmid mix (2.3 µg psPAX2, 0.7 µg pMD2.G, 3 µg pInducer20-ONECUT1) and 7.5 µL Lipofectamine 2000 (Invitrogen, Cat#11668-019) diluted in 250 µL Opti-MEM (Thermo Fisher, Cat#31985-070). Viral supernatants were collected at 24, 36, and 48 h, filtered (0.45 µm PES, Millipore), and fresh medium was added after each harvest. HepG2 and Huh6 cells were infected with fresh viral supernatant and selected with 200 µg/mL G418 (Thermo Fisher, Cat#10131035) for 4-6 days. Stably selected cells were used for Western blot analysis.

Cell cycle analysis

HepG2 pInducer20-ONECUT1 and Huh6 pInducer20-ONECUT1 cells were cultured without doxycycline (DOX-, n = 3) or with 5 µg/ml doxycycline (DOX+, n = 3) for 48 h to induce ONECUT1 overexpression. Approximately 5 × 10^5 cells were collected, washed twice with PBS, and fixed in 1.2 mL of pre-chilled anhydrous ethanol at -20 ° C overnight. After centrifugation (300 x g, 5 min) and PBS wash, cells were resuspended in 100 µL RNase A and incubated at 37 ° C for 30 min, followed by staining with 400 µL PI solution (50 µg/mL) at 4 ° C in the dark for 30 min. Samples were analyzed by flow cytometry, recording propidium iodide (PI) fluorescence with 488 nm excitation.

Apoptosis assays

The apoptosis assay was performed using the Annexin V-FITC/PI Apoptosis Detection Kit (Elabscience, Houston, TX; E-CK-A211). HepG2 pInducer20-ONECUT1 and Huh6 pInducer20-ONECUT1 cells were cultured with or without 5 μg/mL doxycycline (DOX; n=3 each) for 48 hours to induce ONECUT1 overexpression. Cells were then centrifuged at 300 x g for 5 min, washed, and resuspended (~ 5×10^5 cells) in 500 μL of 1× Annexin V Binding Buffer. Annexin V-FITC (5 μL) and PI (5 μL, 50 μg/mL) were added, gently mixed, and incubated at room temperature in the dark for 15-20 min. Samples were analyzed by flow cytometry immediately thereafter.

Mouse experiments

All animal experiments were performed in accordance with protocols approved by the Institutional Animal Care and Use Committee of the University of Hawaii Cancer Center. For this study, wild-type FVB/N mice were obtained from the Jackson Laboratory (Sacramento, CA). Mice at 5–7 weeks of age underwent hydrodynamic tail vein injection (HTVI) to establish the HB model, as described in our earlier work. Once liver tumors reached a size of 4–6 g, the expression of the human tumor suppressor gene ONECUT1 was induced by supplying mice with doxycycline-containing drinking water (ONECUT1-ON), while control mice received regular drinking water without doxycycline (ONECUT1-OFF). The plasmid mixture for injection contained the following amounts: pT3-EF1α-MYC-ΔN90-β-catenin (20 μg), pT3-EF1α-Flag-YAPS127A (20 μg), TRE-ONECUT1-PGK-rTTA (60 μg), and pCMV(CAT)T7-SB100 (4 μg). Doxycycline was administered at a final concentration of 0.467 mg/mL in drinking water. To deplete $CD4^+$ and $CD8^+$ T cells in mice, anti-mouse CD4 monoclonal antibody (clone GK1.5, Purified *in vivo* GOLD™ Functional Grade, Leinco Technologies) and anti-mouse CD8 monoclonal antibody (clone YTS 169, Purified *in vivo* GOLD™ Functional Grade, Leinco Technologies) were administered. Mice received 200 μg of each antibody per mouse via intraperitoneal injection 5 days before the initiation of

doxycycline treatment and again on the day doxycycline water was administered. Control animals received isotype IgG under the same schedule. Both groups were given doxycycline-containing drinking water. After 3 days of doxycycline treatment, mice were sacrificed. Detailed mouse information is provided in Supplemental Table 1. Mice were monitored daily and sacrificed either at predetermined time points or when moribund, as previously reported. Liver samples were collected and processed for hematoxylin and eosin (H&E) staining, immunohistochemistry (IHC), Western blotting (WB), and quantitative RT-PCR (qRT-PCR). Information on antibodies and primers used in IHC, WB, and qRT-PCR assays is summarized in Supplemental Tables 2-4.

For the xenograft model, male NOD/SCID/IL2Rγnull (NSG) mice (5-6 weeks old, Beijing Huafukang Biotechnology Co., Ltd) were subcutaneously inoculated with $5x10^6$ HepG2 pInducer20-ONECUT1 stably transfected cells. When tumors reached a volume of approximately 500 mm^3, mice were randomized into control (DOX-) or treatment (DOX+) groups. Tumors were measured every three days. The tumor volume was calculated as (length $\times$ $width^2$)/2. Tumor growth curves were analyzed using two-way ANOVA, and tumor weights were compared using an unpaired t-test.

Histology, Immunohistochemistry, and Assessment of Mouse Proliferation Rate

Mouse liver tissues were fixed in 10% neutral-buffered formalin overnight at 4 °C, followed by paraffin embedding. Paraffin sections (5 μm) were stained with hematoxylin and eosin (H&E; Thermo Fisher Scientific, Waltham, MA) according to routine protocols to evaluate the histopathological features of hepatocellular lesions in both human and mouse liver samples. For IHC analyses, paraffin sections were first deparaffinized and subjected to heat-induced antigen retrieval in 10 mmol/L sodium citrate buffer (pH 6.0) by boiling for 10 min. After cooling, sections were treated with 5% goat serum together with the Avidin/Biotin blocking kit (Vector Laboratories,

Burlingame, CA) to minimize nonspecific binding. Slides were then incubated overnight at 4 °C with primary antibodies (Supplemental Table 2). Endogenous peroxidase activity was quenched by treatment with 3% hydrogen peroxide in methanol for 20 min. The following day, sections were incubated with species-specific secondary antibodies for 1 h at room temperature. Detection was performed with the Vectastain Elite ABC Kit (Vector Laboratories) and visualized using 3,3′-diaminobenzidine (DAB) as chromogen. Sections were counterstained with hematoxylin. Negative controls were prepared by omitting the primary antibody and incubating only with secondary antibodies. Images were acquired on a Leica DFC295 bright-field microscope equipped with a digital color camera (San Francisco, CA). Hepatocellular proliferation was quantified by determining the Ki-67 labeling index, with at least 2000 nuclei counted per sample[18].

Protein Extraction and Western Blot Analysis

Frozen mouse liver tissues and cultured cell pellets were lysed in Mammalian Protein Extraction Reagent (Thermo Fisher Scientific) supplemented with phosphatase inhibitors. Protein concentrations were quantified using the Bio-Rad Protein Assay Kit (Bio-Rad, Hercules, CA) with bovine serum albumin (BSA) as the calibration standard. Equal amounts of protein were mixed with Tris-Glycine SDS sample buffer (Life Technologies, Carlsbad, CA) and denatured by boiling. Samples were resolved by SDS–polyacrylamide gel electrophoresis (SDS-PAGE) and transferred onto nitrocellulose membranes (Life Technologies) using electroblotting. Membranes were blocked for 1 h in 5% non-fat dry milk, followed by overnight incubation at 4 °C with primary antibodies (Supplemental Table 3). After washing, membranes were incubated with horseradish peroxidase (HRP)-conjugated secondary antibodies (Jackson ImmunoResearch, West Grove, PA; 1:5000 dilution, 30 min). Protein signals were visualized with the SuperSignal West Femto Chemiluminescent Substrate (Pierce, New York, NY).

RNA extraction and quantitative reverse transcription real-time polymerase chain reaction

Total RNA was extracted from HB cell lines or mouse liver tissues using the Quick RNA Miniprep Kit (Zymo Research, Irvine, CA). The RNA was then reverse-transcribed into cDNA using the iScript™ Reverse Transcription Supermix (Bio-Rad, Hercules, CA). Quantitative real-time PCR (qRT-PCR) was performed with TaqMan Universal PCR Master Mix (Thermo Fisher Scientific, Waltham, MA) on a QuantStudio™ 6 Flex or ABI Prism 7000 system (Applied Biosystems). Each 10 μL reaction contained 1 μL of cDNA (100 ng), 5 μL of PCR master mix, 1 μL of primer/probe mix, and 3 μL of distilled water. Cycling conditions were as follows: polymerase activation at 95 °C for 10 min, followed by 40 cycles of denaturation at 95 °C for 15 s and extension at 60 °C for 1 min. Primers used for qRT-PCR are listed in Supplemental Table 4.

RNA sequencing analysis

Total RNA was extracted from HepG2 pInducer20-ONECUT1 cells cultured with or without 5 μg/mL doxycycline (n = 3 per group) using the TRIzol reagent. RNA libraries were prepared with the TruSeq™ RNA Sample Preparation Kit (Illumina) and sequenced on an Illumina HiSeq XTEN/NovaSeq 6000 platform by Majorbio (Shanghai). Raw reads were trimmed and quality-checked with fastp[19], then aligned to the reference genome using HISAT2[20]. Transcript assembly was performed with StringTie[21], and gene abundances were quantified with RSEM[22] as transcripts per million (TPM). Differential expression was analyzed with DESeq2[23]; genes with $|\log2FC| > 2$ and adjusted $P < 0.05$ were considered significant. Gene Set Enrichment Analysis[24] (GSEA) was conducted using the GSEA software, with genes ranked by the Signal2Noise metric. Pathway-specific heatmaps were visualized using the pheatmap package in R.

Statistical analysis

All *in vitro* and *in vivo* data were analyzed using GraphPad Prism version 10.0 (GraphPad Software, San Diego, CA). For *in vitro* experiments and mouse studies, statistical significance was determined using a two-tailed unpaired Student's t-test. Mouse survival data were evaluated by the Kaplan-Meier method and compared with the log-rank (Mantel-Cox) test. All results are reported as mean $\pm$ SD, and a p-value < 0.05 was considered to indicate statistical significance.

Results

Overexpression of ONECUT1 inhibits HB cell growth in culture

As the first step to investigate ONECUT1's role in regulating HB progression, we established a DOX-inducible system where the expression of ONECUT1 could be induced in human HB cells upon adding DOX to the medium (DOX-ONECUT1 cells). Functional analysis revealed that ONECUT1 overexpression inhibited the growth of HepG2 (Fig. 1A, Fig. 1C) and Huh6 (Fig. 1B, Fig. 1D) cells *in vitro*. Cell cycle analysis revealed that ONECUT1 overexpression caused G1 phase arrest in HepG2 cells (Fig. 1E-F). Furthermore, an increased apoptosis rate was noted upon ONECUT1 overexpression (Fig. 1G). Similar results were obtained using Huh6 cells (Sup. Fig. 1).

In summary, our study demonstrates that the overexpression of ONECUT1 in human HB cells inhibits their growth by inducing G1 phase arrest and apoptosis.

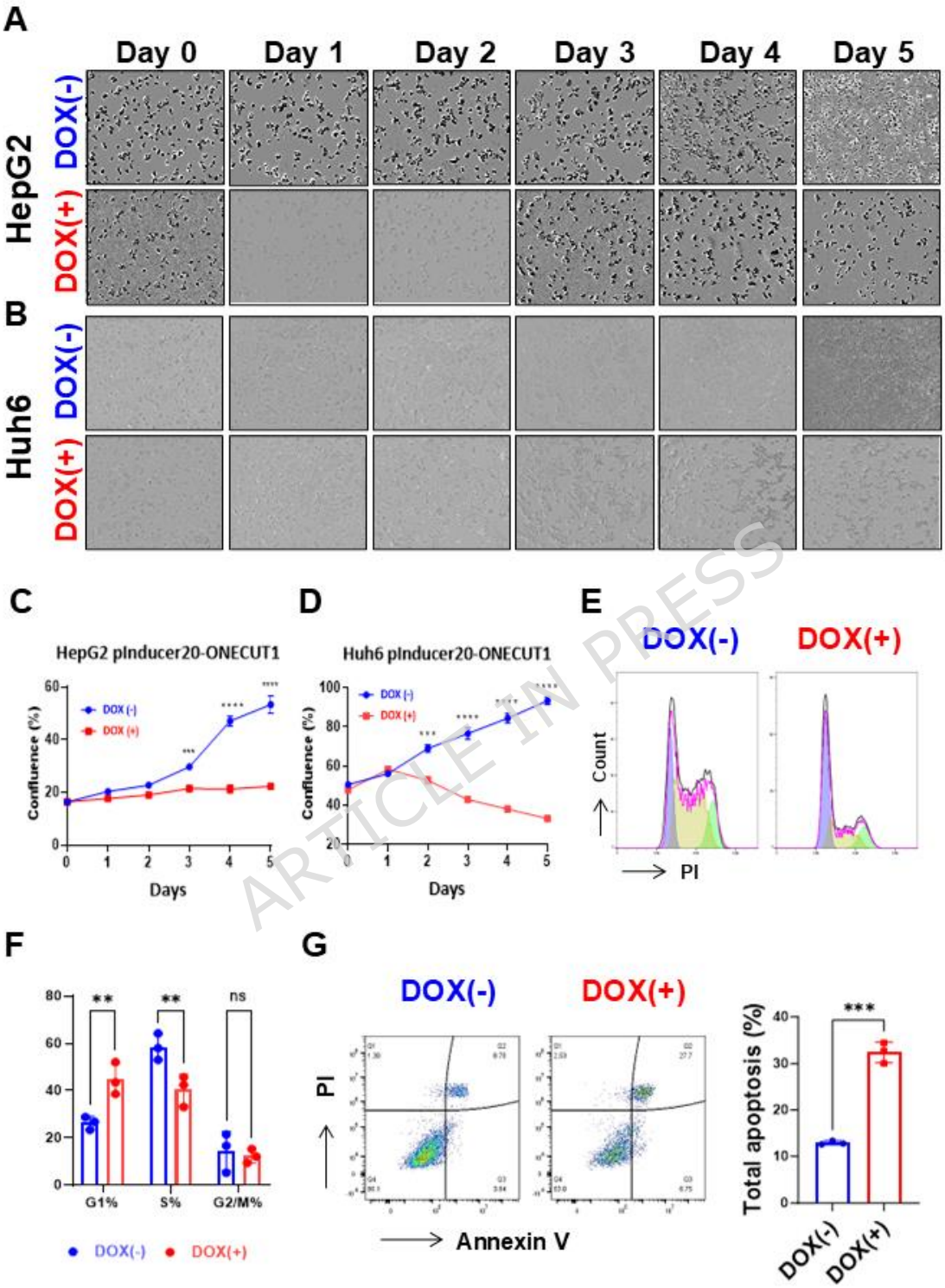

Fig.1

Overexpression of ONECUT1 suppresses HB progression in a xenograft model

Next, we determined whether ONECUT1 overexpression could suppress HB progression in a mouse xenograft model. Thus, we implanted the DOX-ONECUT1 HepG2 cells into the NSG mice, and the mice were initially given regular water. Once the tumor burden was established, we fed the mice with DOX-containing water to induce ONECUT1 expression (Fig. 2A). Notably, overexpression of ONECUT1 markedly inhibited HepG2 progression. In the control group, tumors continued to grow with regular-water feeding. In contrast, DOX-induced ONECUT1 expression in the experimental HepG2 cells suppressed tumor growth (Fig. 2B), resulting in a substantial reduction in tumor volume (Fig. 2C). It is important to note that ONECUT1 overexpression did not induce HB regression, and tumor burden appeared to be stabilized after 6 days of DOX feeding. Histological evaluation showed that ONECUT1 expression was markedly higher in the HepG2 ONECUT1 overexpression group, while HepG2 cells themselves exhibited almost no endogenous ONECUT1 expression (Fig. 2D). In tumor tissues with ONECUT1 overexpression, the Ki67-positive rate was significantly lower compared to the non-overexpression group (Fig. 2E), whereas the cleaved caspase-3 (CC3)-positive rate was significantly higher than that in the non-overexpression group (Fig. 2F). Thus, the results indicate that ONECUT1 inhibits cell proliferation and induces apoptosis in HepG2 cells.

Altogether, the data show that ONECUT1 overexpression suppresses HB progression but does not cause tumor regression in the xenograft model.

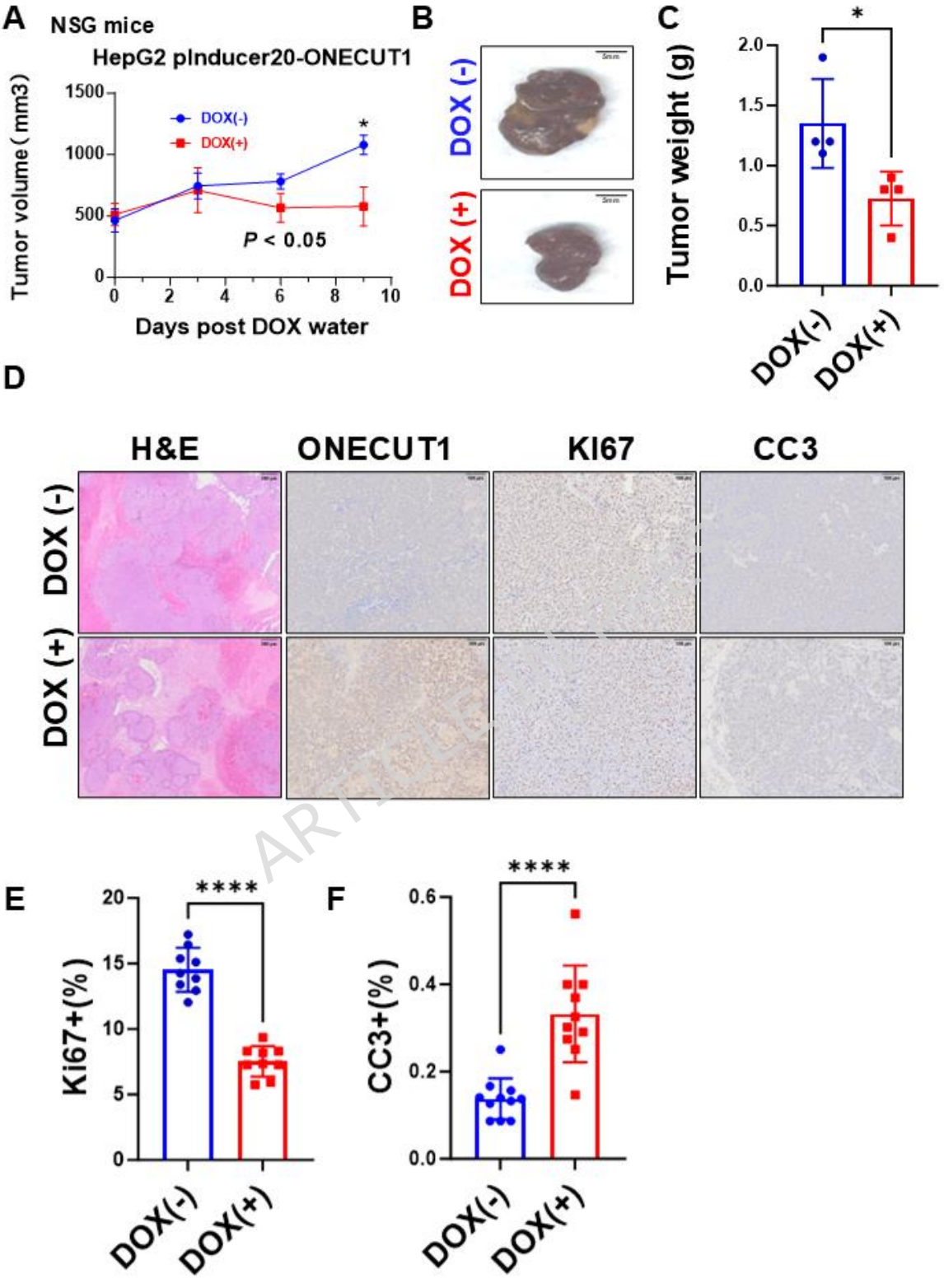
A
NSG mice
HepG2 pInducer20-ONECUT1
Tumor volume (mm3)
1500
1000
500
0
DOX(-)
DOX(+)
*
P < 0.05
0
2
4
6
8
10
Days post DOX water
B
DOX (-)
DOX (+)
C
Tumor weight (g)
2.0
1.5
1.0
0.5
0.0
*
DOX(-)
DOX(+)
D
H&E
ONECUT1
KI67
CC3
DOX (-)
DOX (+)
E
Ki67+(%)
20
15
10
5
0
****
DOX(-)
DOX(+)
F
CC3+(%)
0.6
0.4
0.2
0.0
****
DOX(-)
DOX(+)

Fig.2

Overexpression of ONECUT1 induces tumor regression in the YAP/β-Catenin murine HB model

Next, we investigated whether ONECUT1 overexpression hampers HB progression *in vivo*. For this purpose, we applied the YAP/β-Catenin-driven murine HB model. In addition, we generated the pT3-TRE-ONECUT1 construct, which allows the expression of ONECUT1 upon DOX-treatment in mouse hepatocytes. Thus, the *pT3-EF1α-YAPS127A*, *pT3-EF1α-ΔN90-β-Catenin* (with MYC-tag), and *pT3-TRE-ONECUT1* plasmids, together with the pCMV(CAT)T7-SB100 constructs, were co-injected into the mouse liver (YAP/β-Catenin/TRE-ONECUT1) (Fig. 3A). Mice were fed with regular water and monitored for liver tumor growth as a palpable abdominal mass (Fig. 3B). Once liver tumor lesions were detected, a cohort of mice was harvested as pre-treatment cohort (Fig. 3B). The remaining mice were randomly separated into two cohorts: one cohort of mice were continued with regular water, and the second cohort of mice were fed with DOX-water, allowing the expression of ONECUT1 in already-formed HB cells (Fig. 3B). Mice were harvested at 1, 2, 3, 7 days, or long term (8 weeks) post-DOX-water feeding. As expected, ONECUT1 expression was rapidly induced and its overexpression could be readily detected after 1-3 days of DOX-feeding (Fig. 3C and 3D).

We found that ONECUT1 overexpression strongly suppressed YAP/β-Catenin HB progression. liver weight (LW) and the liver weight-to-body weight ratio (LW/BW), used as measures of tumor burden, showed a decrease compared with pre-DOX controls. This reduction achieved statistical significance by days 2 and 3 (Fig. 3E and 3F). Thus, the data indicate that tumors began to regress at these early time points. This trend continued, leading to prolonged mouse survival (Fig. 3G). In the long-term DOX-on mice, only a few small tumor nodules were noted on the liver surface, confirming that ONECUT1 overexpression led to HB regression (Fig. 3H).

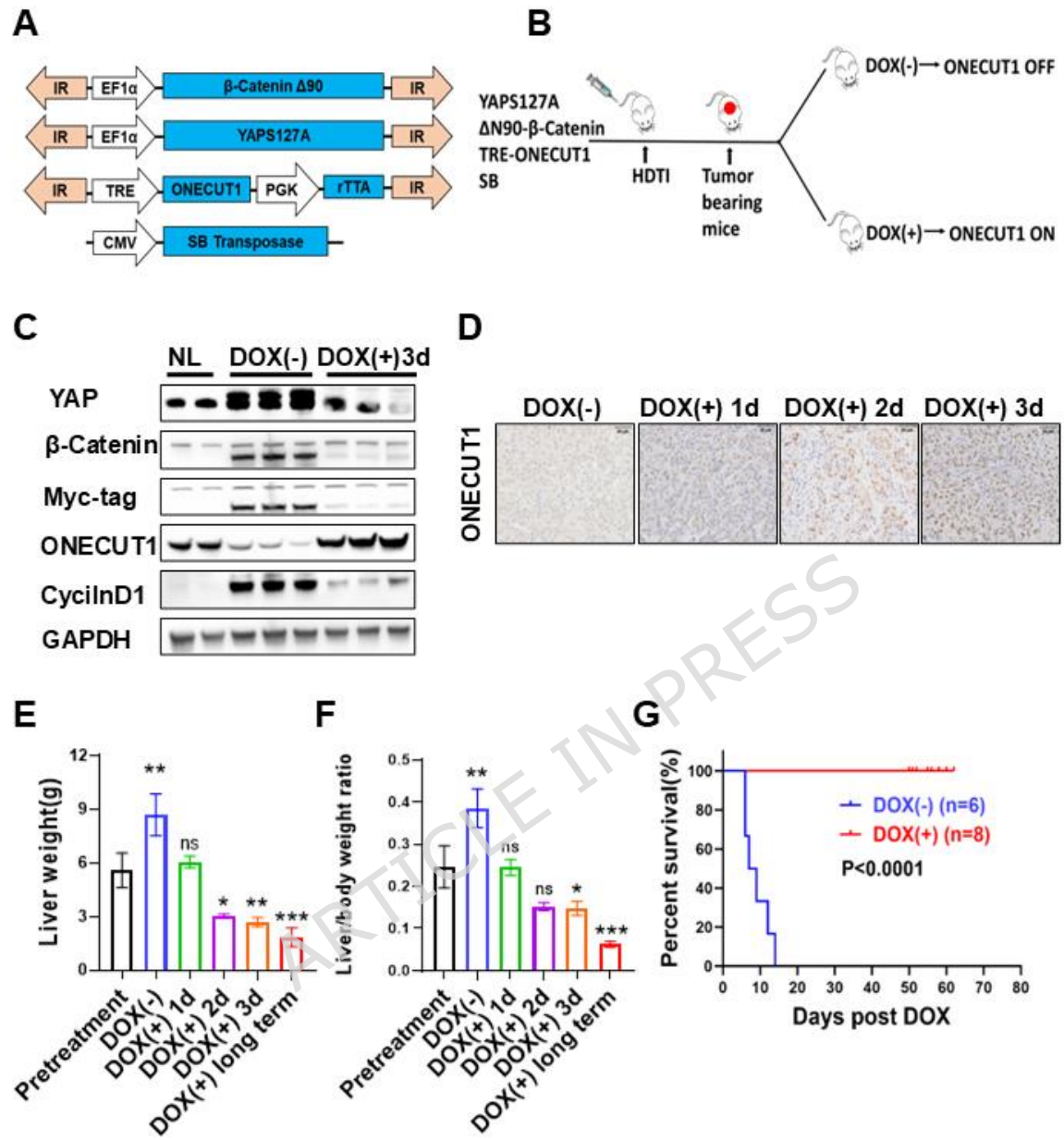

Fig.3

Histological evaluation revealed that, in the pretreatment group, lesions appeared as solid sheets of small tumor cells with high nuclear-to-cytoplasmic ratios (Fig. 4A–C). In the absence of ONECUT1 induction, tumors continued to progress, occupying large areas of the liver parenchyma and developing prominent central necrotic regions (N), a characteristic feature of rapidly proliferating HB with insufficient vascularization (Fig. 4D–F). Following DOX-induced ONECUT1 overexpression, the tumors underwent extensive necrotic and apoptotic cell death. By day 3, the lesions exhibited coagulative necrosis, with pale, faint nuclei and eosinophilic cytoplasm, forming classic “ghost cells”, accompanied by early inflammatory cell infiltration (Fig. 4G–I). Notably, the necrotic regions were bordered by non-neoplastic parenchyma, indicating complete loss of viable tumor cells, in contrast to hypoxia-induced necrosis typically surrounded by proliferating tumor tissue. By day 7 after ONECUT1 induction, the necrotic tumor tissue had been completely replaced by collagen-rich scar tissue (S), frequently accompanied by dystrophic calcifications and foreign-body-type multinucleated giant cells, reflecting active tissue replacement and clearance of cellular debris (Fig. 4J–L).

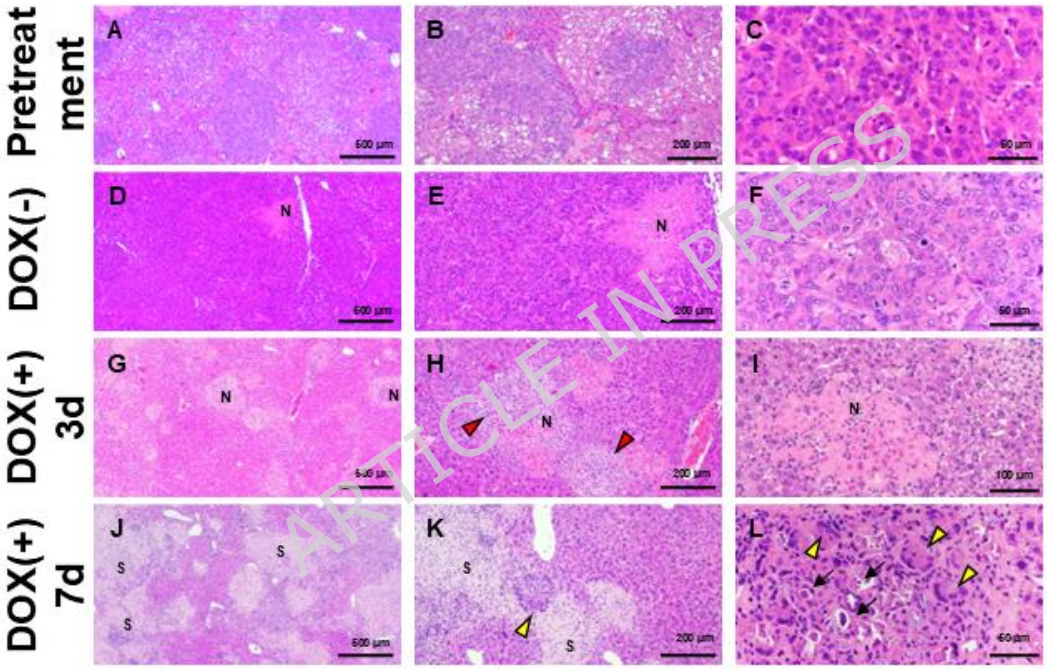

Fig.4

Immunohistochemical (IHC) staining showed that, consistent with the *in vitro* studies, ONECUT1 overexpression significantly inhibited HB cell proliferation (Fig. 5A). At 3 days post ONECUT1 induction, these areas were also strongly positive for CC3 (Fig. 5B). In contrast, livers from DOX (−) control mice exhibited minimal CC3 immunoreactivity. The results were consistent with our studies using HepG2 cells that ONECUT1 overexpression induces apoptosis in HB cells. The liver parenchyma exhibited a strong fibroblastic response circumscribing the necrotic areas, as demonstrated by pronounced α-smooth muscle actin (α-SMA) immunolabeling (Fig. 5C), which was largely absent in DOX (-) control mice. A robust macrophage infiltration characterized the lesions, as revealed by pronounced immunoreactivity for F4/80 (Fig. 5D), whereas only sparse $F4/80^+$ cells were detected in DOX (-) livers. Furthermore, a mild to moderate infiltration of $CD4^+$ and $CD8^+$ T cells could be detected (Fig. 5E and Sup. Fig. 2), while DOX (-) controls displayed minimal T cell infiltration. At the later time point, specifically 7 days after DOX feeding, a decrease in CC3 and α-SMA immunoreactivity could be observed, which could be attributed to tissue replacement by fibrous scars (Fig. 5B and 5C). This process was paralleled by an increase in infiltration of the scar tissue by $CD4^+$ cells and a decrease in the macrophage compartment, as indicated by F4/80 staining, compared with livers at 3 days after ONECUT1 overexpression (Fig. 5D and 5E).

In summary, overexpression of ONECUT1 leads to tumor regression in the YAP/β-Catenin murine HB model.

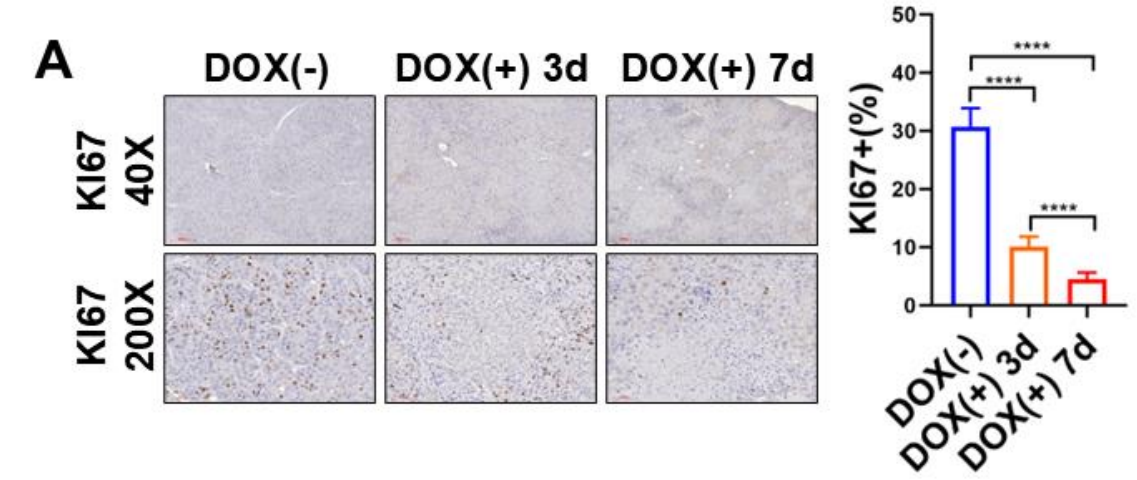

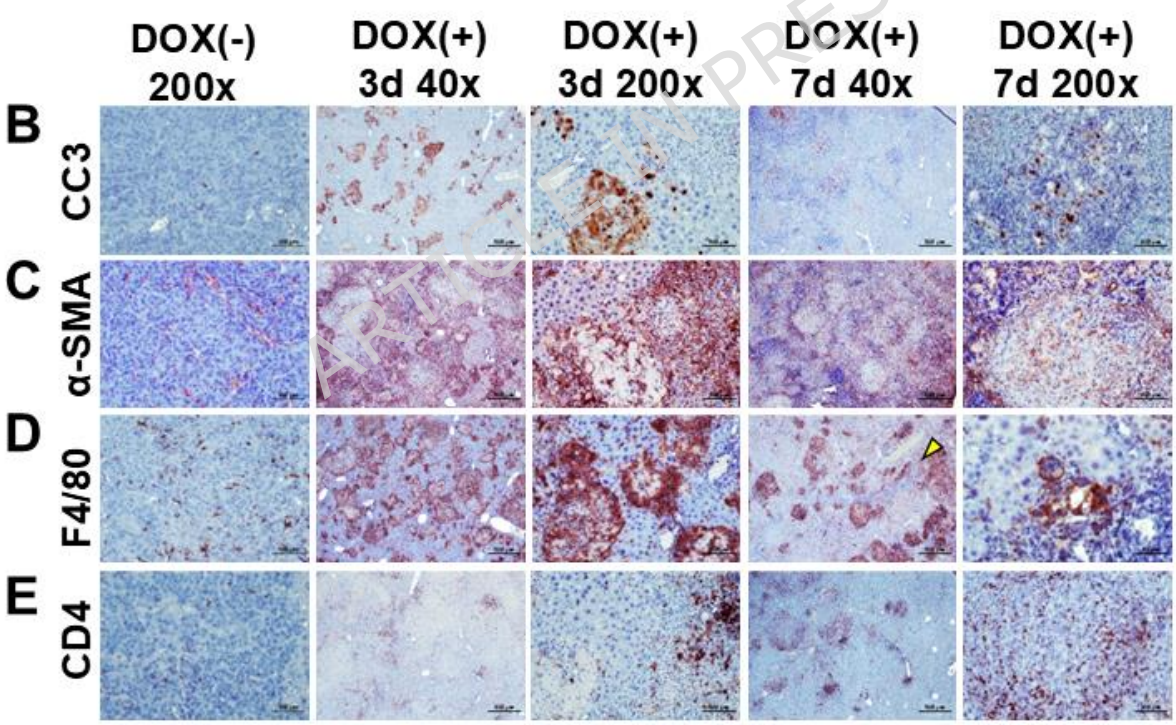

Fig.5

T-cell depletion partly inhibits YAP/β-Catenin HB regression induced by ONECUT1 overexpression

Clearly, a markedly different outcome characterized the xenograft HB model (Fig. 2) and the oncogene-induced murine HB model following forced overexpression of ONECUT1 (Fig. 3 and 4). In immune-deficient mice implanted with HepG2 cells, ONECUT1 overexpression suppressed tumor progression but did not trigger regression. In contrast, ONECUT1 overexpression in YAP/β-Catenin-driven mouse HB cells caused extensive tumor cell death and ultimately tumor regression in immunocompetent mice. A key distinction between the two systems lies in their immune microenvironments.

Thus, we determined whether T-cell depletion inhibits ONECUT1 overexpression induced YAP/β-Catenin HB regression. For this purpose, we hydrodynamically injected YAP/β-Catenin/TRE-ONECUT1 plasmids into mice. Mice were fed with regular water and monitored for liver tumor growth. Once the liver tumor growth was detected, mice were treated with an anti-CD4/8 antibody, or control IgG. Five days after treatment, a cohort of mice was switched to DOX-water and treated with another dose of IgG or an anti-CD4/8 antibody. Another group of mice continued to be fed regular water and treated with another dose of IgG or an anti-CD4/8 antibody. Three days after the DOX-water treatment, all mice were harvested (Fig. 6A). We found that the anti-CD4/8 treatment had no effect on LW or LW/BW of the DOX(-) mice (Fig. 6B and 6C). This is consistent with the observation that there are few tumor-infiltrating CD4 and CD8 T cells in YAP/β-Catenin lesions. Therefore, one would not expect that depleting CD4 and CD8 T cells would affect YAP/β-Catenin tumor progression. In contrast, in the DOX(+) groups, LW and LW/BW were significantly higher in anti-CD4/8 antibody treated mice, indicating that depletion of T cells partially inhibits tumor regression induced by ONECUT1 overexpression in YAP/β-Catenin mice (Fig. 6B and 6C). Histologically, HB lesions from anti-IgG-treated mice showed significant CD4 and CD8 T cell infiltration, whereas those from anti-CD4/8 antibody-treated mice showed few such cells (Fig. 6D).

In summary, the data indicate that tumor infiltrating T cells facilitate HB regression driven by ONECUT1 overexpression.

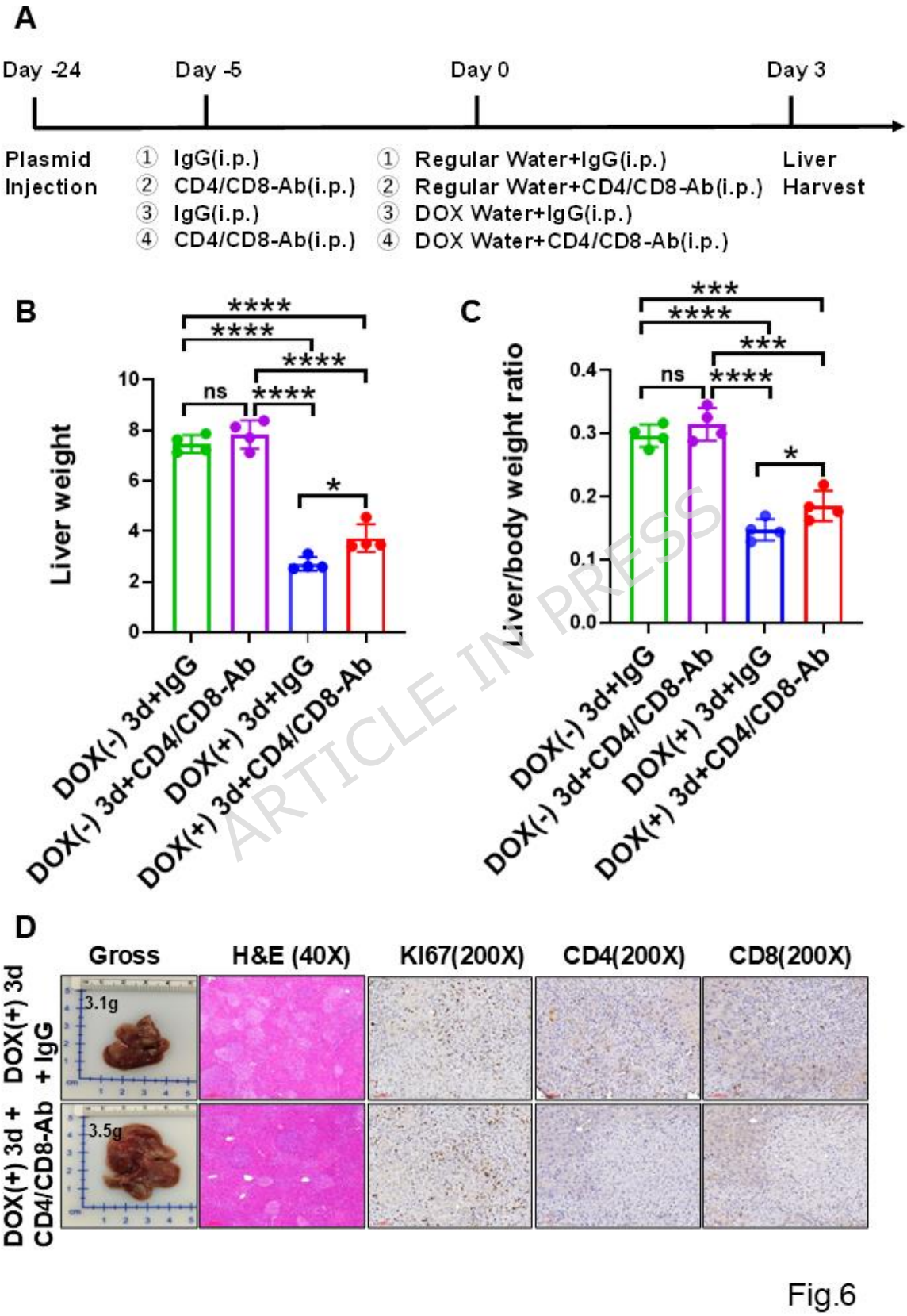

Fig.6

ONECUT1 overexpression affects multiple pathways in HB cells

Finally, to investigate the molecular mechanisms by which ONECUT1 overexpression promotes HB regression, we analyzed the genes regulated by ONECUT1 in HepG2 cells. In brief, DOX-ONECUT1 HepG2 cells were treated with DOX to induce ONECUT1 expression; subsequently, the control and DOX treated cells were subjected to RNA-seq. The Volcano plot showed ONECUT1 overexpression upregulated 2408 genes and downregulated 1017 genes (Fig. 7A). GSEA analysis revealed that ONECUT1 overexpression significantly downregulated the cell cycle, mitotic spindle, and DNA replication pathways (Fig. 7B), consistent with the *in vitro* and *in vivo* studies. Heatmap analysis showed that ONECUT1 overexpression was associated with marked downregulation of key cell cycle regulators, including CDK1, CDK6, CDC20, CDC25, and E2F1 (Fig. 7C), as well as upregulation of genes associated with apoptosis (Sup. Fig. 3). Importantly, ONECUT1 overexpression led to the upregulation of genes involved in antigen processing and presentation (Fig. 7B), such as HLA-B and HLA-G (Fig. 7D).

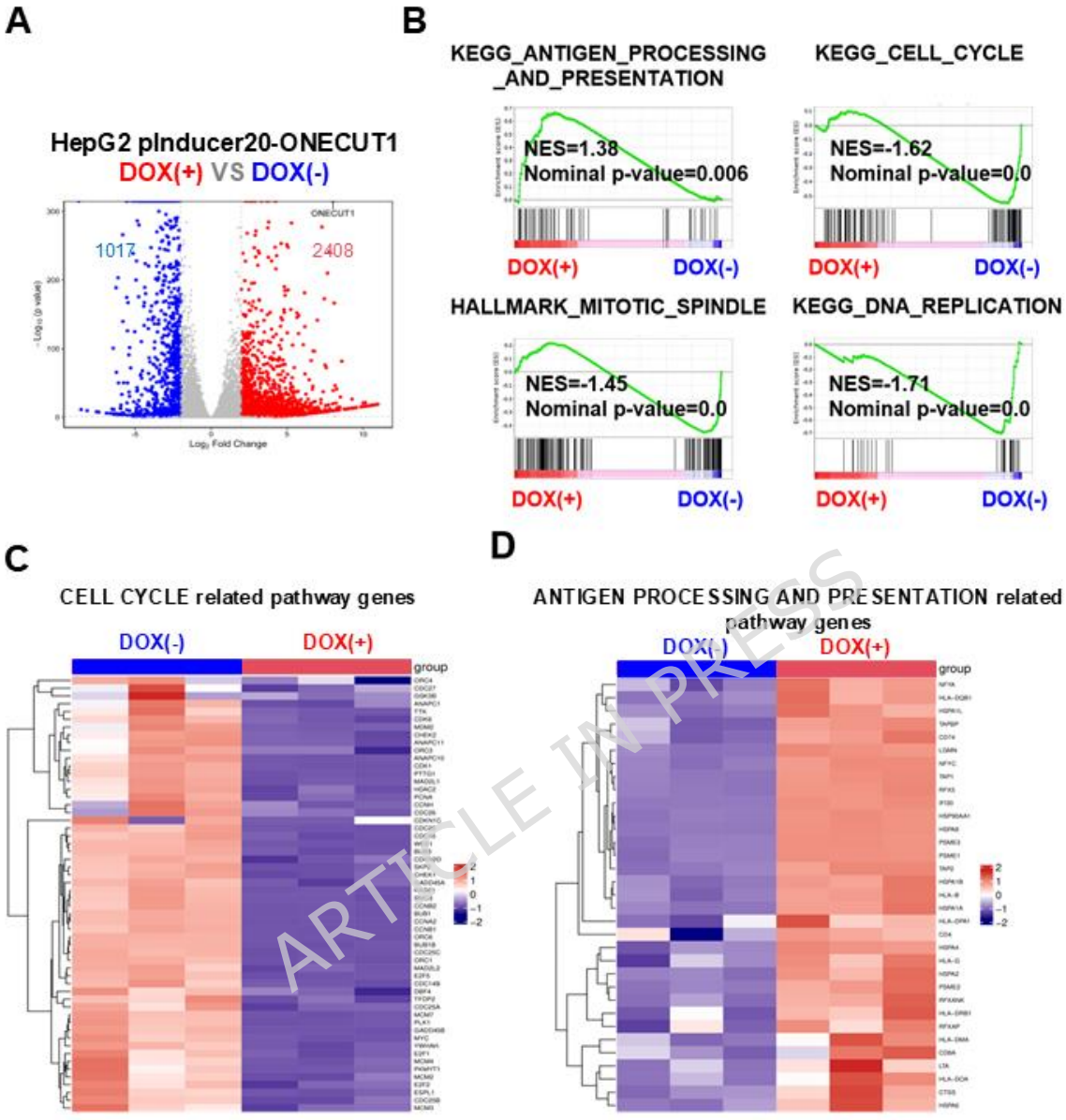

Fig.7

In addition, 16 cytokines were found to be dysregulated by ONECUT1 in HepG2 HB cells (Sup. Table 5). Therefore, we focused on genes that have been implicated in modulating the tumor immune microenvironment (TIME) and whose up- or downregulation is consistent with findings reported in previous studies. Among them, we found a marked upregulation of *CXCL16* and *IL16* upon ONECUT1 overexpression (Fig. 8A), both of which have been reported to promote lymphocyte infiltration within the tumor microenvironment[25, 26]. *CCL20*, which has been previously reported to be associated with tumor-promoting functions[27], was found to be downregulated by ONECUT1 induction in HepG2 cells (Fig. 8A). To strengthen the relevance of these findings *in vivo*, we performed qRT-PCR analysis of these cytokines in ONECUT1-overexpressing YAP/β-Catenin HB lesions. Consistent with the *in vitro* data, *Cxcl16* and *Il16* expression levels were significantly elevated in tumors from ONECUT1 induced YAP/β-Catenin mice (Fig. 8B). In contrast, while *Ccl20* expression was markedly reduced in HepG2 cells, no significant change was observed in the mouse tumors.

In summary, gene expression analysis revealed that ONECUT1 overexpression in HepG2 cells leads to significant transcriptional reprogramming. CXCL16 and IL16 might represent cytokines that might mediate ONECUT1 induced HB tumor microenvironment changes.

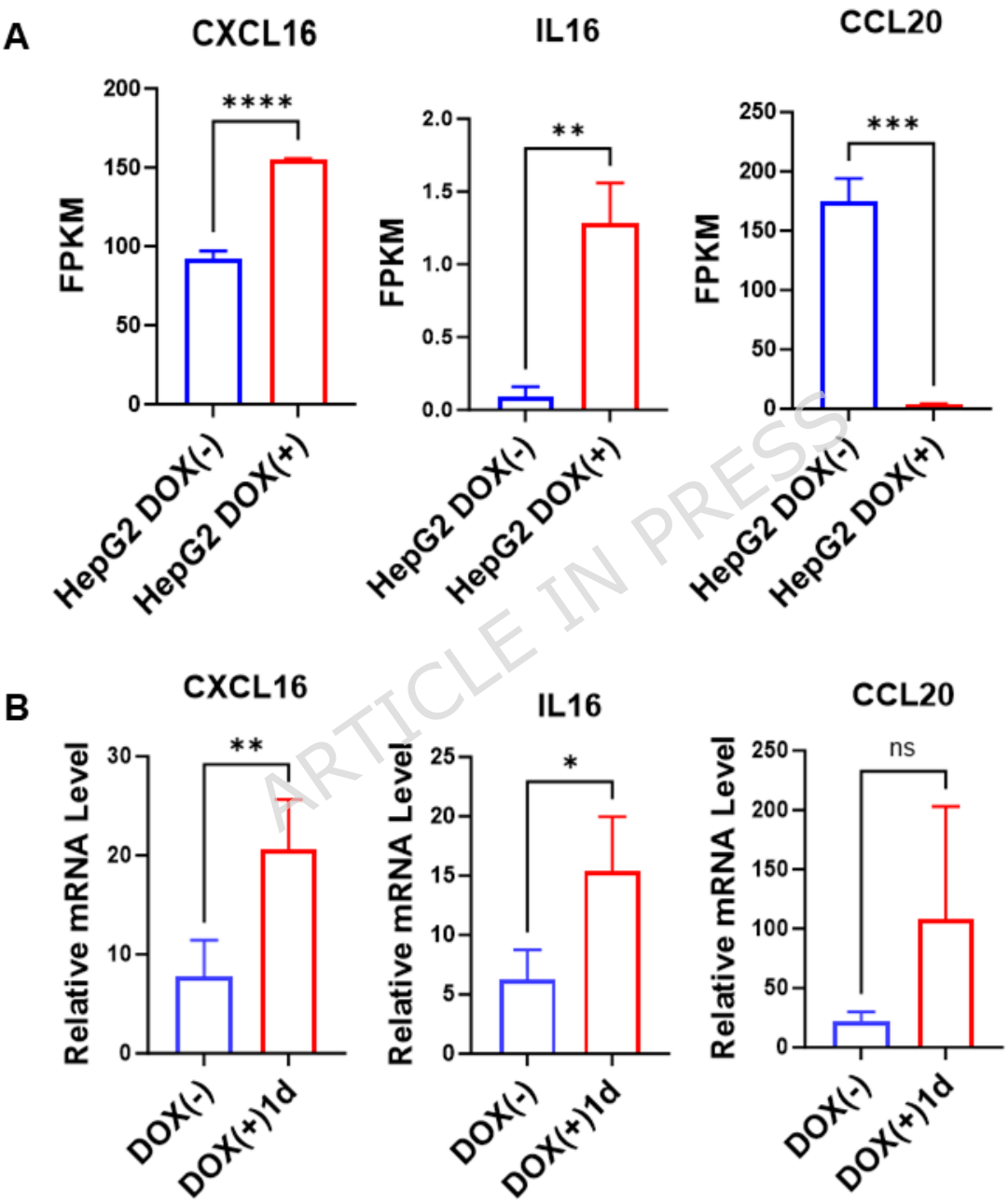

Fig.8

Discussion

In the present study, we demonstrated that the overexpression of ONECUT1 can significantly induce regression of established HB lesions, highlighting its potent antitumor activity. These findings position ONECUT1 as a highly promising therapeutic target for HB. Furthermore, we conducted a systematic investigation into the mechanisms underlying ONECUT1's role in the progression of HB.

First, RNA-seq analysis further revealed that the cell cycle pathway was significantly downregulated upon ONECUT1 overexpression in HepG2 cells, including key genes such as CDK6[28, 29]. Consistent with this finding, cell cycle analysis showed that HB cell lines underwent G1 phase arrest, supporting the notion that ONECUT1 suppresses cell cycle-related genes and inhibits cell proliferation. Similarly, in the YAP/β-catenin/AIO-ONECUT1 mouse model treated with doxycycline, ONECUT1 overexpression reduced Cyclin D1 expression, a well-known regulator of the G1 phase[29]. Furthermore, our data show that increased CC3 expression, as well as genes associated with the apoptosis pathway, accompanied ONECUT1 induction. Collectively, these findings indicate that ONECUT1 overexpression inhibits HB progression by inducing cell cycle arrest and triggering apoptosis.

Of note, in a subcutaneous tumor model, ONECUT1 overexpression inhibited tumor growth but did not completely eradicate the tumor lesions. In contrast, in immunocompetent mice, DOX-induced ONECUT1 forced induction resulted in rapid and complete tumor regression. This discrepancy prompted us to investigate the role of the immune system in the antitumor effects of ONECUT1. When $CD4^+$ and $CD8^+$ T cells were depleted using antibodies, tumor regression was suppressed. These results suggest that the inhibitory effect of ONECUT1 on tumor cells is not solely due to its direct suppression of tumor cell proliferation but also involves activation of the

immune system to eliminate tumor cells, leading to a complete response (tumor-free status) comparable to that observed in clinical settings. Interestingly, RNA-seq analysis revealed that ONECUT1 upregulated the MHC-I antigen presentation pathway in HepG2 cells. Of note, we observed a similar upregulation of MHC-I in YAP/β-Catenin HB mouse lesions, occurring 2 days after ONECUT1 overexpression, just before extensive tumor cell death was detected in these mice (Supplementary Figure 4). Given that low MHC-I expression enables tumor cells to evade immune surveillance[30, 31], this upregulation may enhance tumor immunogenicity by increasing their visibility to cytotoxic T cells, thereby promoting immune-mediated elimination. Importantly, MHC-I downregulation can sometimes be therapeutically restored to enhance antitumor immunity[32]. Thus, ONECUT1 overexpression may restore MHC-I expression on tumor cells, effectively "flagging" them for recognition and elimination by immune cells, resulting in immune-dependent clearance.

To further investigate the molecular mechanisms by which ONECUT1 modulates the TIME, we analyzed the cytokines which are deregulated by ONECUT1 in HepG2 cells and cross validated a set of selected genes using ONECUT1 overexpressed mouse HB tissues. Based on these analyses, we found that CXCL16 and IL16 are potential cytokines regulated by ONECUT1 that may modulate the tumor microenvironment (TME), which is recognized as a critical determinant of tumor progression[33, 34]. CXCL16 acts as a chemokine that recruits immune cells such as T cells, macrophages, neutrophils, and monocytes across various disease contexts[35]. In several tumor models, elevated CXCL16 expression has been shown to chemoattract CXCR6-expressing lymphocytes, including activated $CD8^+$ T cells and natural killer (NK) cells, thereby enhancing antitumor immune responses and cytotoxic activity[25, 36]. IL16, also known as lymphocyte chemoattractant factor (LCF)[37], has likewise been shown to promote antitumor immunity in mouse tumor models[26]. Exogenous IL16 administration facilitates Th1 cell-macrophage crosstalk by

inhibiting glutamine catabolism in $CD4^+$ T cells, increasing IFN-γ production, enhancing $CD8^+$ T cell infiltration, and improving responses to immune checkpoint blockade. Clearly, future studies are required to define the functional roles of CXCL16 and IL16 in HB progression. A similar experimental strategy could be applied to address this question. Specifically, CXCL16 or IL16 could be cloned into the pT3-TRE vector and co-injected with YAP/β-catenin into the mouse liver. Expression of CXCL16 or IL16 could then be induced in HB-bearing mice through DOX administration in drinking water. This approach would allow investigation of the effects of cytokine overexpression on HB progression, with particular emphasis on alterations in the TIME.

Hydrodynamic injection–based liver cancer models have been successfully generated in multiple mouse strains including C57BL/6 and FVB[38]. Although tumor initiation driven by oncogenic events is largely conserved across strains, genetic background may influence the TIME[39]. Further experiments using other genetic background, such as C57BL/6, will be helpful to validate the conclusion that ONECUT1 overexpression induces HB regression.

Overall, our study reveals that ONECUT1 plays a dual role in HB biology. It inhibits cell proliferation by suppressing key drivers of cell cycle progression and enhances the immune system's ability to recognize tumor cells. This effect is achieved by upregulating genes involved in antigen processing and presentation, especially MHC-I molecules. Therefore, activating ONECUT1 could be an effective strategy to control the cell cycle and a promising therapeutic approach to increase tumor immunogenicity. Our findings further support the development of ONECUT1 agonists as a novel treatment strategy for patients with HB.

Figure legends

Figure 1. Overexpression of ONECUT1 inhibits the proliferation of hepatoblastoma cell lines.

(A) HepG2 pInducer20-ONECUT1 cells were seeded and cultured either without DOX (DOX−) or with 5 μg/mL DOX (DOX+). Cell proliferation was monitored daily using the Incucyte system. (B) Huh6 pInducer20-ONECUT1 cells were cultured under the same conditions. (C, D) Quantification of cell confluence for HepG2 (C) and Huh6 (D) pInducer20-ONECUT1 cells in the DOX− and DOX+ groups over 5 consecutive days. (E) Cell cycle analysis. (F) Quantification of cell cycle distribution is shown in (E). Statistical significance was determined by a two-tailed unpaired Student's t-test. (G) Apoptosis analysis. Statistical significance was determined by a two-tailed unpaired Student's t-test. Data are presented as mean ± SD. ns, not significant; **P < 0.01; ***P < 0.001; ****P < 0.0001.

Figure 2. Overexpression of ONECUT1 suppresses hepatoblastoma growth in NSG mice.

(A) Tumor growth curves of subcutaneous xenografts in NSG mice inoculated with HepG2 pInducer20-ONECUT1 cells. When tumor volume reached 500 mm^3, mice were randomized into control (DOX−) or treatment (DOX+) groups, and tumor size was measured every 3 days. Two-way ANOVA was used for comparing tumor growth curves. (B) Representative tumor images. (C) Tumor weight analysis. Statistical significance was determined by a two-tailed unpaired Student's t-test. (D) H&E and IHC staining for ONECUT1, Ki67, and CC3. (E) Quantification of Ki67-positive cells. Statistical significance was determined by a two-tailed unpaired Student's t-test. (F) Quantification of CC3-positive cells. Statistical significance was determined by a two-tailed unpaired Student's t-test. Data are presented as mean ± SD. *P < 0.05; ****P < 0.0001.

Figure 3. Overexpression of ONECUT1 inhibits YAPS127A/ΔN90-β-catenin driven hepatocarcinogenesis in FVB/N mice.

(A) Schematic representation of the plasmid constructs used in the study: EF1α-driven ΔN90-β-catenin and YAPS127A, TRE-ONECUT1 with rTTA, and SB transposase. (B) Cartoon diagram of the hydrodynamic tail-vein injection (HTVI) procedure used to deliver the plasmid mixture into FVB/N mouse hepatocytes and experimental timeline: mice were allowed to develop palpable liver tumors before switching to DOX-containing drinking water to induce ONECUT1 expression. (C) Western blot showing protein expression in liver tumors under indicated conditions. ONECUT1 is robustly induced after DOX treatment. Myc-tag indicates ΔN90-β-catenin expression, and Cyclin D1 expression is markedly decreased following ONECUT1 overexpression. GAPDH serves as loading control. (D) IHC staining for ONECUT1 in mice subjected to pretreatment and ONECUT1 overexpression for 1, 2, and 3 days. Scale bar: 50 μm (200×). (E) Liver weights. (F) Liver-to-body weight ratio. (G) Survival of YAPS127A/ΔN90-β-catenin mice with or without DOX. (H) Representative gross images of tumor-bearing livers before treatment, DOX−, and at indicated time points after DOX induction (1 day, 3 days, 7 days, and 8 weeks). Liver weight is shown in the upper left corner of the image. Statistical significance was determined by a two-tailed unpaired Student's t-test. Data are presented as mean ± SD. ns, not significant; *P < 0.05; **P < 0.01; ***P < 0.001.

Figure 4. Overview of liver lesions developing in YAPS127A/ΔN90-β-catenin mice.

(A–C) In the pretreatment group, lesions appear as solid masses consisting of small cells with prominent nuclei. (D–F) Lesions became more aggressive, as assessed by the presence of necrotic areas (N), and occupied the liver parenchyma when mice were not subjected to ONECUT1 overexpression. (G–I) As a result of ONECUT1 forced induction, lesions underwent necrotic and apoptotic cell death. (I) Early necrosis characterized these lesions: nuclei were still visible but pale, and the cytoplasm was eosinophilic due to coagulation necrosis, resulting in "ghost cells". An inflammatory-like reaction (red arrowheads in H) begins to resorb the dead cells. Necrosis is surrounded by non-neoplastic tissue, distinct from hypoxic tumor-center necrosis

shown in (D, E). (J–L) Seven days after ONECUT1 overexpression, lesions were replaced by collagenous scars (S). Due to lesion size, fibrotic tissue replaced necrotic areas. Dystrophic calcifications (black arrows) formed from calcium release by dead cells and were resolved by foreign body giant cells (yellow arrowheads). Liver lesions are shown at three magnifications: 40× (A, D, G, J), 100× (B, E, H, K), and 400× (C, F, I, L). Scale bars: 500 µm (A, D, G, J), 200 µm (B, E, H, K), 50 µm (C, F, I, L).

Figure 5. Overview of YAPS127A/ΔN90-β-catenin liver lesions following ONECUT1 overexpression.

(A) Representative immunohistochemical staining for Ki67 in liver sections from YAP/β-catenin/TRE-ONECUT1 mice without DOX, and at 3 and 7 days after DOX induction. ONECUT1 overexpression markedly reduced Ki67-positive proliferating tumor cells. Quantification of Ki67 positive nuclei is shown on the right. Data are presented as mean ± SD. ****P < 0.0001 (unpaired two-tailed Student's t-test). Scale bars: 200 µm (40×) and 50 µm (200×). (B–E) Immunostaining of serial liver sections from the same mice for (B) CC3, (C) α-SMA, (D) F4/80, and (E) CD4 in DOX (−) controls and at 3 and 7 days after DOX induction. (B) CC3 positive apoptotic cells were abundant at 3 days and reduced by 7 days, consistent with extensive early apoptosis, whereas CC3 immunoreactivity was minimal in DOX (−) livers. (C) α-SMA staining indicates pronounced fibroblastic activation surrounding necrotic areas at 3 days, which decreased at 7 days during tissue replacement with fibrous scars, with little α-SMA signal detected in DOX (−) controls. (D) Robust macrophage (F4/80) infiltration was observed at 3 days and diminished at 7 days, with occasional multinucleated giant macrophages (yellow arrowhead), while DOX (−) livers exhibited only sparse $F4/80^+$ cells. (E) Infiltration of $CD4^+$ T cells increased from 3 to 7 days following ONECUT1 induction and a mild to moderate infiltration of $CD8^+$ T cells in DOX-induced lesions (Sup. Fig. 2), which was largely absent in DOX (−) controls. Scale bars: 200 µm (40×) and 50 µm (200×).

Figure 6. Depletion of T cells partially inhibits ONECUT1-induced hepatoblastoma regression in YAPS127A/ΔN90-β-catenin mice.

(A) Experimental design. FVB/N mice were hydrodynamically injected with YAPS127A/ΔN90-β-catenin/TRE-ONECUT1 plasmids on Day −24. On Day −5, mice received i.p. injections of control IgG or anti-CD4 plus anti-CD8 antibodies (CD4/CD8-Ab). On Day 0, DOX treatment was initiated to induce ONECUT1 expression or regular water as a DOX (−) control, accompanied by the same antibody regimen. Mice were sacrificed on Day 3 after DOX induction or the corresponding time point in DOX (−) groups. Four experimental groups were included: DOX (+) + IgG, DOX (+) + CD4/CD8-Ab, DOX (−) + IgG, and DOX (−) + CD4/CD8-Ab. (B–C) Quantification of liver weight (B) and liver-to-body weight ratio (C) Under DOX (+) conditions, T-cell depletion significantly attenuated ONECUT1-induced tumor regression (*P < 0.05). In contrast, under DOX (−) conditions, CD4/CD8 depletion did not significantly affect liver weight or liver-to-body weight ratio. Statistical significance was determined by a two-tailed unpaired Student's t-test. Data are presented as mean ± SD. ns, not significant; *P < 0.05; ***P < 0.001; ****P < 0.0001. (D) Representative gross liver morphology and histological analyses. Images from DOX (+) groups are shown. H&E staining (40×) shows larger tumor burden in CD4/CD8-depleted mice. Ki67 immunostaining (200×) indicates higher proliferation in CD4/CD8-Ab–treated livers. CD4 and CD8 immunostaining (200×) confirms successful T-cell depletion.

Figure 7. Genes and pathways induced by ONECUT1 in hepatoblastoma cells.

(A) Volcano plot showing differentially expressed genes (DEGs) upon ONECUT1 overexpression in HepG2 cells. A total of 2,408 genes were upregulated and 1,017 genes were downregulated (|log2FC| > 2, adjusted p-value < 0.05). ONECUT1 is highlighted, confirming robust overexpression. (B) GSEA pathway analysis. Significantly enriched pathways included KEGG_ANTIGEN_PROCESSING_AND_PRESENTATION, KEGG_CELL_CYCLE,

HALLMARK_MITOTIC_SPINDLE, and KEGG_DNA_REPLICATION. NES, normalized enrichment score. (C) Heatmap of cell cycle–related genes, showing that most genes were downregulated after DOX-induced ONECUT1 overexpression, indicating suppression of cell cycle progression. (D) Heatmap of antigen processing and presentation–related genes, showing that most genes were upregulated after DOX-induced ONECUT1 overexpression, suggesting that ONECUT1 enhances antigen presentation.

Figure 8. ONECUT1 overexpression upregulates cytokines associated with immune cell recruitment in hepatoblastoma.

(A) RNA-seq analysis of HepG2 pInducer20-ONECUT1 cells cultured with or without DOX induction. Expression levels (FPKM) of *CXCL16*, *IL16*, and *CCL20* are shown. ONECUT1 overexpression significantly increased CXCL16 and IL16 expression while markedly suppressing CCL20 expression (**P < 0.01, ***P < 0.001, and ****P < 0.0001; unpaired two-tailed Student's t-test). (B) Quantitative RT-PCR validation of *Cxcl16*, *Il16,* and *Ccl20* mRNA levels in YAP/β-catenin/TRE-ONECUT1 mouse livers without DOX and 1 day after DOX induction. (*P < 0.05, **P < 0.01, ns = not significant; unpaired two-tailed Student's t-test). Data are presented as mean ± SD.

References

1. Pio L, O'Neill AF, Woodley H, Murphy AJ, Tiao G, Franchi-Abella S, Fresneau B, Watanabe K, Alaggio R, Lopez-Terrada D, Hiyama E, Branchereau S. Hepatoblastoma. Nat Rev Dis Primers 2025;11:36.
2. Xing H, Yang C, Tan B, Zhang M. Incidence trends and predictive model of hepatic malignant tumors in children: a population-based study. Am J Transl Res 2022;14:7268-89.
3. Nussbaumer G, Benesch M. Hepatoblastoma in molecularly defined, congenital diseases. Am J Med Genet a 2022;188:2527-35.
4. Garg A, Wu TC. A Long-Term Survivor of Trisomy 18. Cureus 2024;16:e51491.
5. Zhang Y, Solinas A, Cairo S, Evert M, Chen X, Calvisi DF. Molecular Mechanisms of Hepatoblastoma. Semin Liver Dis 2021;41:28-41.
6. Hu H, Zhang W, Zhang Y, Gao Y, Zhi T, Li F, Li J, Gu H, Liao R, Wu R, Huang D. Individualized chemotherapy and efficacy analysis of hepatoblastoma in children. Pediatr Blood Cancer 2024;71:e30693.
7. Wang Y, Chen H, Liu Y, Xiao H, Wang X, Zhong Z, Gao P, Zhang Z, She J, Liu J, Huang L, Jiang H. Treatment optimization for recurrent hepatoblastoma: retrospective study from a hepatoblastoma cohort in Southern China. Pediatr Surg Int 2022;38:1031-9.
8. Zhang W, Meyfeldt J, Wang H, Kulkarni S, Lu J, Mandel JA, Marburger B, Liu Y, Gorka JE, Ranganathan S, Prochownik EV. beta-Catenin mutations as determinants of hepatoblastoma phenotypes in mice. J Biol Chem 2019;294:17524-42.
9. Tao J, Calvisi DF, Ranganathan S, Cigliano A, Zhou L, Singh S, Jiang L, Fan B, Terracciano L, Armeanu-Ebinger S, Ribback S, Dombrowski F, et al. Activation of beta-catenin and Yap1 in human hepatoblastoma and induction of hepatocarcinogenesis in mice. Gastroenterology 2014;147:690-701.
10. Tachmatzidi EC, Galanopoulou O, Talianidis I. Transcription Control of Liver Development. Cells 2021;10.
11. Jiang K, Jiao Y, Liu Y, Fu D, Geng H, Chen L, Chen H, Shen X, Sun L, Ding K. HNF6 promotes tumor growth in colorectal cancer and enhances liver metastasis in mouse model. J Cell Physiol 2019;234:3675-84.
12. Yuan XW, Wang DM, Hu Y, Tang YN, Shi WW, Guo XJ, Song JG. Hepatocyte nuclear factor 6 suppresses the migration and invasive growth of lung cancer cells through p53 and the inhibition of epithelial-mesenchymal transition. J Biol Chem 2013;288:31206-16.

13. Pekala KR, Ma X, Kropp PA, Petersen CP, Hudgens CW, Chung CH, Shi C, Merchant NB, Maitra A, Means AL, Gannon MA. Loss of HNF6 expression correlates with human pancreatic cancer progression. Lab Invest 2014;94:517-27.

14. Zhu H, Mi Y, Jiang X, Zhou X, Li R, Wei Z, Jiang H, Lu J, Sun X. Hepatocyte nuclear factor 6 inhibits the growth and metastasis of cholangiocarcinoma cells by regulating miR-122. J Cancer Res Clin Oncol 2016;142:969-80.

15. Liao W, Zhang Y, Wang J, Cui G, Evert M, Xu M, Wu Y, Wang X, Deng S, Song X, Monga SP, Zhao J, et al. beta-Catenin regulates distinct pathways from YAP and suppresses ONECUT1 to drive hepatoblastoma development in mice and humans. Hepatology 2025.

16. Wang X, Zhou Y, Zhang S, Farrar C, Xie X, Li J, Zhang SM, Zhang Z, Yonemura A, Haynes JT, Feng X, Shang R, et al. Targeting mTORC2-dependent AKT/FOXO1/RNF125 signaling exploits a therapeutic vulnerability in c-MET-activated and β-catenin-mutated hepatocellular carcinoma. Hepatology (Baltimore, Md.) 2025:10-1097.

17. Cui G, Zhou Y, Liao W, Cossu E, Evert M, Zhang S, Wang J, Deng S, Yonemura A, David L, Xu M, Doumergue JM, et al. Inhibition of GSK3 and TSC2 Mediates the Oncogenic Activity of AKT in Hepatocellular Carcinoma. Cancer Res 2025.

18. Kitson S, Sivalingam VN, Bolton J, McVey R, Nickkho-Amiry M, Powell ME, Leary A, Nijman HW, Nout RA, Bosse T, Renehan AG, Kitchener HC, et al. Ki-67 in endometrial cancer: scoring optimization and prognostic relevance for window studies. Modern pathology : an official journal of the United States and Canadian Academy of Pathology, Inc 2017;30:459-68.

19. Chen S, Zhou Y, Chen Y, Gu J. fastp: an ultra-fast all-in-one FASTQ preprocessor. Bioinformatics 2018;34:i884-90.

20. Kim D, Langmead B, Salzberg SL. HISAT: a fast spliced aligner with low memory requirements. Nat Methods 2015;12:357-60.

21. Pertea M, Pertea GM, Antonescu CM, Chang TC, Mendell JT, Salzberg SL. StringTie enables improved reconstruction of a transcriptome from RNA-seq reads. Nat Biotechnol 2015;33:290-5.

22. Li B, Dewey CN. RSEM: accurate transcript quantification from RNA-Seq data with or without a reference genome. Bmc Bioinformatics 2011;12:323.

23. Love MI, Huber W, Anders S. Moderated estimation of fold change and dispersion for RNA-seq data with DESeq2. Genome Biol 2014;15:550.

24. Subramanian A, Tamayo P, Mootha VK, Mukherjee S, Ebert BL, Gillette MA, Paulovich A, Pomeroy SL, Golub TR, Lander ES, Mesirov JP. Gene set enrichment analysis: a

knowledge-based approach for interpreting genome-wide expression profiles. Proc Natl Acad Sci U S a 2005;102:15545-50.

25. Matsumura S, Wang B, Kawashima N, Braunstein S, Badura M, Cameron TO, Babb JS, Schneider RJ, Formenti SC, Dustin ML, Demaria S. Radiation-induced CXCL16 release by breast cancer cells attracts effector T cells. J Immunol 2008;181:3099-107.

26. Wen Z, Liu T, Xu X, Acharya N, Shen Z, Lu Y, Xu J, Guo K, Shen S, Zhao Y, Wang P, Li S, et al. Interleukin-16 enhances anti-tumor immune responses by establishing a Th1 cell-macrophage crosstalk through reprogramming glutamine metabolism in mice. Nat Commun 2025;16:2362.

27. Kadomoto S, Izumi K, Mizokami A. The CCL20-CCR6 Axis in Cancer Progression. Int J Mol Sci 2020;21.

28. Tadesse S, Yu M, Kumarasiri M, Le BT, Wang S. Targeting CDK6 in cancer: State of the art and new insights. Cell Cycle 2015;14:3220-30.

29. Bertoli C, Skotheim JM, de Bruin RA. Control of cell cycle transcription during G1 and S phases. Nat Rev Mol Cell Biol 2013;14:518-28.

30. Cordon-Cardo C, Fuks Z, Drobnjak M, Moreno C, Eisenbach L, Feldman M. Expression of HLA-A,B,C antigens on primary and metastatic tumor cell populations of human carcinomas. Cancer Res 1991;51:6372-80.

31. Dhatchinamoorthy K, Colbert JD, Rock KL. Cancer Immune Evasion Through Loss of MHC Class I Antigen Presentation. Front Immunol 2021;12:636568.

32. Taylor BC, Balko JM. Mechanisms of MHC-I Downregulation and Role in Immunotherapy Response. Front Immunol 2022;13:844866.

33. Kwee SA, Tiirikainen M. Beta-catenin activation and immunotherapy resistance in hepatocellular carcinoma: mechanisms and biomarkers. Hepatoma Res 2021;7.

34. Lodetti Zangrandi G, Tirpanlar D, Pastore M, Soldani C, Lleo A, Raggi C. Tumor microenvironment highlighting tumor-associated macrophages and immune cells. Hepatoma Research 2023;9:32.

35. Palakurthi B, Fross SR, Guldner IH, Aleksandrovic E, Liu X, Martino AK, Wang Q, Neff RA, Golomb SM, Lewis C, Peng Y, Howe EN, et al. Targeting CXCL16 and STAT1 augments immune checkpoint blockade therapy in triple-negative breast cancer. Nat Commun 2023;14:2109.

36. Hojo S, Koizumi K, Tsuneyama K, Arita Y, Cui Z, Shinohara K, Minami T, Hashimoto I, Nakayama T, Sakurai H, Takano Y, Yoshie O, et al. High-level expression of chemokine

CXCL16 by tumor cells correlates with a good prognosis and increased tumor-infiltrating lymphocytes in colorectal cancer. Cancer Res 2007;67:4725-31.

37. Ogasawara H, Takeda-Hirokawa N, Sekigawa I, Hashimoto H, Kaneko Y, Hirose S. Inhibitory effect of interleukin-16 on interleukin-2 production by CD4+ T cells. Immunology 1999;96:215-9.

38. Chen X, Calvisi DF. Hydrodynamic transfection for generation of novel mouse models for liver cancer research. The American journal of pathology 2014;184:912-23.

39. Huang P, Rodriguez-Matos FJ, Qi J, Trehan R, Myojin Y, Zhu XB, Greten TF, Ma C. Hepatic immune environment differences among common mouse strains in models of MASH and liver cancer. JHEP reports : innovation in hepatology 2025;7:101380.